ISSN: 2641-1784

Research Article

Advance in Environmental Waste Management & Recycling

Removal of polyaromatics from textile industry using La /ZnO nanocomposite

Delia Teresa Sponza* , **Rukiye Oztekin**[a]

[a]*Department of Environmental Engineering, Engineering Faculty, Dokuz Eylül University, Tınaztepe Campus, 35160, Buca/İzmir, Turkey*

***Corresponding author**
Prof. Dr. Delia Teresa Sponza, Department of Environmental Engineering, Engineering Faculty, Dokuz Eylül University, Tınaztepe Campus, 35160, Buca/İzmir, Turkey.

Submitted: 19 July 2021; **Accepted**: 26 July 2021; **Published**: 03 Aug 2021

Citation: *Delia Teresa Sponza and Rukiye Oztekin (2021). Removal of polyaromatics from textile industry using La /ZnO nanocomposite. Adn Envi Was Mana Rec, 4 (2):108-126.*

Abstract

The effects of the type and amount of loadings on the photocatalytic activity of Ln/ ZnO were studied and the results were compared with pure ZnO. The textile wastewaters (TW) could not be treated effectively with concentional treatment processes due to high polyphenols and colour content. In this study, La/ZnO nanocomposite was used for the photocatalytic oxidation of pollutant parameters [COD components (COD_{total}, $COD_{dissolved}$, COD_{inert}), polyaromatic amines and color] from the textile effluent wastewaters (TW) at different operational conditions such as, at increasing photooxidation times (5 min, 15 min, 30 min, 60 min, 80 min and 100 min), at diferent La mass ratios (0.5wt% , 1wt%, 1.5wt%, 2wt%), at different La-ZnO photocatalyst concentrations (1, 5, 15, 30 and 45 mg/L), under 10, 30, 50 and 100 W ultraviolet (UV) irradiations, respectively. The maximum COD_{total}, COD_{inert}, total aromatic amines (TAAs) and color photooxidation yields were 99%, 92%, 98% and 99% respectively, under the optimized conditions, at 30 mg/L La/ZnO nanocomposite with a La mass ratio of 1.5 wt% under 50 W UV light, after 60 min photooxidation time, at 25oC. The photooxidation yields of 2-methoxy-5-methylaniline (MMA), 2,4-diaminoanisole(DAA); 4,40-diamino diphenyl ether (DDE), o-aminoazotoluene (OAAT), and 4-aminoazobenzol (AAB) polyaromatic amines were > 82%. The pollutants of textile industry wastewater were effectively degraded with lanthanum doped ZnO nanocomposite.

Keywords: Lanthanum doped ZnO (La-ZnO) nanocomposite, Photooxidation, Polyaromatic amines, Ultraviolet (UV) light irradiation.

Introductıon

Textile industry is one of those industries that consume large amounts of water in the manufacturing process and, also, discharge great amounts of effluents with synthetic dyes to the environment causing public concern and legislation problems[1]. Synthetic dyes that make up the majority (60–70%) of the dyes applied in textile processing industries are considered to be serious health risk factors. Apart from the aesthetic deterioration of water bodies, many colorants and their breakdown products are toxic to aquatic life and can cause harmful effects to humans [2-5]. Several physico-chemical and biological methods for dye removal from wastewater have been investigated and seem that each technique faces the facts of technical and economical limitations [6-8]. The traditional physical, chemical and biologic means of wastewater treatment often have little degradation effect on this kind of pollutants. On the contrary, the technology of nanoparticulate photodegradation has been proved to be effective to them. Compared with the other conventional wastewater treatment means, this technology has such advantages as: (1) wide application, especially to the molecule structure-complexed contaminants which cannot be easily degraded by the traditional methods; (2) the nanoparticles itself have no toxicity to the health of our human livings and (3) it demonstrates a strong destructive power to the pollutants and can mineralize the pollutants into carbondioxide (CO2) and water (H2O) [9].

Semiconductor photocatalysis is an advanced oxidation process (AOP) for the treatment of wastewater streams Mills and Hunte, 1997 [10]. Zinc oxide (ZnO), a II–VI compound semiconductor with a wide direct band gap (3.37 eV) and a large exciton binding energy (60 meV) at room temperature, has attracted increasing attention due to its excellent electrical and optoelectronic properties and wide potential applications in photocatalysts, [11,12]. As a photocatalyst, the destruction ability of ZnO and ZnO based materials starts with absorption of light energy equal or greater than the band-gap energy and continues with the generation of electron–hole pairs. Then, these charge carriers can be separately trapped by the oxygen (O2) and surface hydroxyl (OH) groups to

produce primary oxidizing species; hydroxyl radicals (OH●). The subsequent attacks of the radicals to surface adsorbed pollutants yield mineralized species. The higher efficiency of ZnO has been reported in several studies such as photocatalytic oxidation of phenol 2-phenly phenol acid red 18 remazol brilliant blue R, remazol black B, reactive blue 221 and reactive blue 222 [13-16].

In order to reduce the recombination rate of ZnO in the photocatalytic processes some alkaline and rare earth metal atoms can be doped on the surface of the semiconductors, which have been shown to reduce band gap energy and improve charge separation between photogenerated electrons and holes [17]. Recently found 90% monocrotophos removal efficiency during photooxidation at a power of 64 W using 25 g/L La-ZnO with a La mass ratio of 0.8 wt% after 120 min. It was found that La-doped ZnO showed higher photocatalytic activity in the degradation of monocrotophos as compared to that of pure ZnO and TiO2[18]. Metal dopants have also been used to improve the morphology and photocatalytic activity of nano-doped ZnO[19-22]. When 0.6wt% La mass ratio was doped into ZnO, more surface defects are produced, which hindered the recombination of photo-induced electron–hole pairs [23,24]. investigated the photoooxidation of Rhodamine B and Acid-Red 18 from textile wastewaters (TW) using nano-ZnO[25-26]. The photodegradation studies performed with La doped ZnO to remove some dyes from TW are limited only with few studieswere used nano La doped ZnO to treat the Rhodamine B, Metilen blue and azo dyes[27-28]. No study was found investigating the pollutants (COD, the flavonols and polyaromatic amines from TW with La doped ZnO.

Therefore, in the present study, La-ZnO nanocomposite was used for the photocatalytic oxidation of pollutant parameters [COD components (COD_{total}, $COD_{dissolved}$, COD_{inert}), flavonols (kaempferol, quercetin, patuledin, rhamnetin and rhamnazin), polyaromatic amines (2-methoxy-5-methylaniline, 2,4-diaminoanisole, 4,40-diamino diphenyl ether, o-aminoazotoluene, and 4-aminoazobenzol) and color] from the TW at different operational conditions such as, at increasing photooxidation times (5 min, 15 min, 30 min, 60 min, 80 min and 100 min), at diferent La mass ratios (0.5wt% , 1wt%, 1.5wt%, 2wt%), at different La doped-ZnO photocatalyst concentrations (1, 5, 15, 30 and 45 mg/L), at different pH ranges (4, 6, 8, 10) under 10, 30, 50 and 100 W UV light irradiations, respectively.

Materıal and Methods

Raw wastewater

The characterization of raw TW was given in

Table 1. Characterization values of TW at pH=5.7 (n=3, mean values ± SD). (SD: standard deviation; n: the repeat number of experiments in this study).

Parameters	Values		
	Minimum	Medium	Maximum
pH	5.00 ± 0.18	5.27 ± 0.19	6.00 ± 0.21
DO (mg/L)	1.30 ± 0.05	1.40 ± 0.05	1.50 ± 0.05
ORP (mV)	85.00 ± 2.98	106.00 ± 3.71	128.00 ± 4.48
TSS (mg/L)	285.00 ± 9.98	356.00 ± 12.46	430.00 ± 15.05
TVSS (mg/L)	192.00 ± 6.72	240.00 ± 8.40	290.00 ± 10.15
COD_{total} (mg/L)	931.70 ± 32.61	1164.60 ± 40.76	1409.20 ± 49.32
$COD_{dissolved}$ (mg/L)	770.40 ± 26.96	962.99 ± 33.71	1165.22 ± 40.78
TOC (mg/L)	462.40 ± 16.18	578.00 ± 20.23	700.00 ± 24.50
BOD5 (mg/L)	251.50 ± 8.80	314.36 ± 11.00	380.38 ± 13.31
$BOD5/COD_{dis}$	0.26 ± 0.01	0.33 ± 0.012	0.40 ± 0.014
Total N (mg/L)	24.80 ± 0.87	31.00 ± 1.09	37.51 ± 1.31
NH_4-N (mg/L)	1.76 ± 0.06	2.20 ± 0.08	2.66 ± 0.09
NO_3-N (mg/L)	8.00 ± 0.28	10.00 ± 0.35	12.10 ± 0.42
NO_2-N (mg/L)	0.13 ± 0.05	0.16 ± 0.06	0.19 ± 0.07
Total P (mg/L)	8.80 ± 0.31	11.00 ± 0.39	13.30 ± 0.47
PO_4^{-P} (mg/L)	6.40 ± 0.22	8.00 ± 0.28	9.68 ± 0.34
SO_4^{-2} (mg/L)	1248.00 ± 43.70	1560.00 ± 54.60	1888.00 ± 66.10
Color (1/m)	70.90 ± 2.48	88.56 ± 3.10	107.20 ± 3.75
Flavonols (mg/L)	30.9 ± 1.08	38.6 ± 1.35	46.1 ± 1.61

Flavonols			
Kaempferol	4.2 ± 0.20	5.7 ± 0.2	7.2 ± 0.3
Quercetin	7.3 ± 0.26	9.2 ± 0.32	11.1 ± 0.4
Patuledin	8.3 ± 0.30	10.3 ± 0.36	12.2 ± 0.43
Rhamnetin	6.0 ± 0.21	7.2 ± 0.25	8.4 ± 0.3
Rhamnazin	5.1 ± 0.18	6.15 ± 0.22	7.2 ± 0.25
TAAs (mg benzidine/L)	891.84 ± 31.21	1038 ± 36.33	1183.8 ± 41.43
Polyaromatics			
2-methoxy-5-methylaniline	128.5 ± 4.5	134.6 ± 4.71	140.6 ± 4.92
2,4-diaminoanisole	250.2 ± 8.76	275.8 ± 9.7	301.3 ± 10.6
4,40-diamino diphenyl ether	146.54 ± 5.13	156.0 ± 5.5	165.4 ± 5.8
o-aminoazotoluene	265.4 ± 9.3	293.6 ± 10.3	321.7 ± 11.3
4-aminoazobenzol	101.2 ± 3.54	178 ± 6.23	254.8 ± 8.92

Chemical structure of flavonols and poliaromatics present in the TW

The structure of flavonols in the TW was shown in The structure of polyaromatics in the TW was given

Chemical structure of flavonoids hemical structure of flavonoids

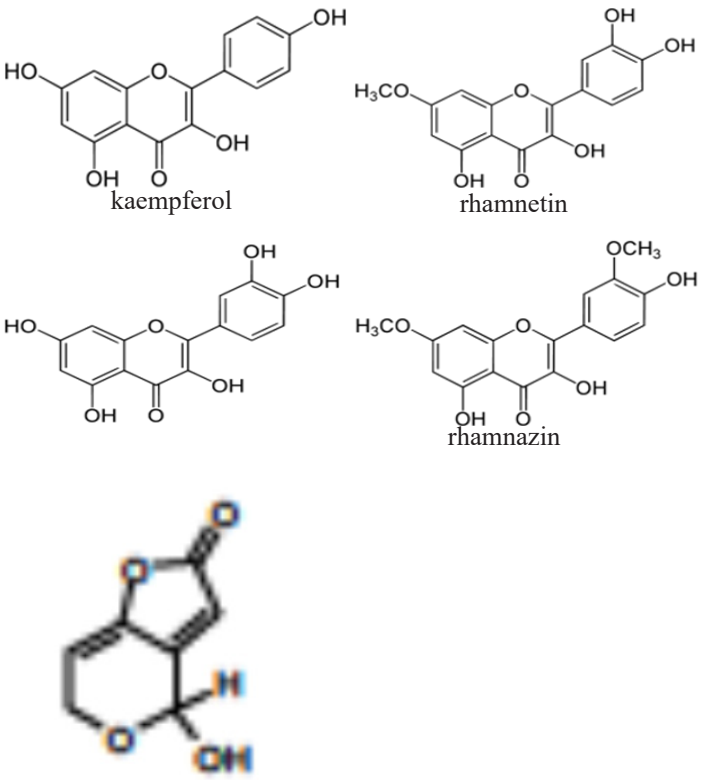

Figure 1: Chemical structure of flavonoids in the TW.

Chemical structure of polyaromatics Chemical structure of polyaromatics

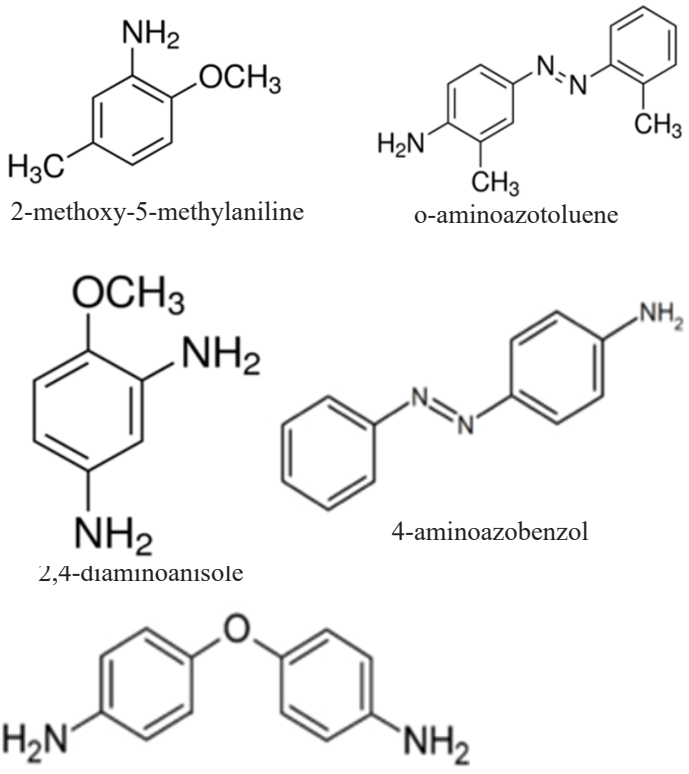

Figure 2: Chemical structure of polyaromatics in the TW

Preparation of photocatalysts

La-doped ZnO nano particles were prepared by co-precipitation method using zinc nitrate hexahydrate [$Zn(NO_3)_2.6H_2O$] (Analytical grade, Merck) and lanthanum nitrate hexahydrate [$La(NO_3)_3$•$6H_2O$] (Sigma, Aldrich) as the precursors of zinc and lanthanum, respectively. $Zn(NO3)_2.6H_2O$ and sodium carbonate anhydrous (Na2CO3) were dissolved separately in double distilled H2O to obtain 0.5 mol/L solutions. Lanthanum nitrate in the

required stoichiometry was slowly added into the above solution and a white precipitate was obtained. The precipitate was filtered, repeatedly rinsed with distilled H_2O and then washed twice with ethanol. The resultant solid product was dried at 100°C for 12 h and calcined at 300°C for 2 h. The doped La mass ratios of lanthanum are expressed as wt%.

X-Ray Diffraction (XRD) Analysis

XRD patterns of the samples are going to carry out using a D/Max-2400Rigaku X-ray powder diffractometer operated in the reflection mode with Cu Ka (λ = 0.15418 nm) radiation through scan angle (2θ) from 20o to 80o.

Scanning Electron Microscopy (SEM) Analysis

The morphological structures of the La-ZnO nanocomposites before photocatalytic degradation with UV light irradiations and after photocatalytic degradation with UV by means of a SEM.

Fourier transform infrared spectroscopy (FTIR) Analysis

The FTIR spectra of La, ZnO and La-ZnO samples were measured with FTIR spectroscopy measurements.

Photocatalytic Degradation Reactor

A 2 L cylinder quartz glass reactor was used for the photodegradation experiments in the TW under different UV powers, at different operational conditions. 1000 mL TW was filled for experimental studies and the photocatalyst were added to the cylinder quartz glass reactors. The UV-A lamps were placed to the outside of the photo-reactor with a distance of 3 mm. The photocatalytic reactor was operated with constant stirring (1.5 rpm) during the photocatalytic degradation process

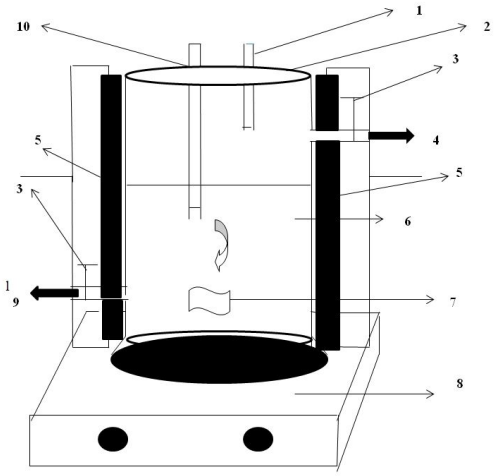

Figure 3: Photodegradation experimental scheme (1: thermometer, 2: teflon proofed cover, 3: proofed tap, 4: gas sampling inlet, 5: UV light sources (OSRAM Germicidal Hg lamb, 30 W UV-C lamb), 6: 1000 mL kuvars glass reactor, 7: magnetic fish, 8: magnetic stirrer, 9: liquid sampling inlet, 10: pH meter

10 mL of the reacting solution were sampled and centrifugated (at 10000 rpm) at different time intervals. The UV irradiation treatments were created using one or three UV-A lamp emitting in the 350–400 nm range (λ_{max} = 368 nm; FWHM = 17 nm; Actinic BL TL-D 18W, Philips).

Used Chemicals

$Zn(NO_3)_2.6H_2O$ (Analytical Grade, Merck, Germany) and $La(NO_3)_3 \bullet 6H_2O$ (Analytical grade, Merck, Germany) were used as zinc and lanthanum sources, respectively. Na_2CO_3 was purchased from Merck (Analytical grade). Helium, He(g) (GC grade, 99.98%) and nitrogen, N2(g) (GC grade, 99.98%) was purchased from Linde, (Germany). 2-methoxy-5-methylaniline (99%), 2,4-diaminoanisole (99%), 4,40-diamino diphenyl-ether (99%), o-aminoazotoluene (99%), 4-aminoazobenzol (99%) were purchased from Aldrich, (Germany).

Analytical Methods

pH, T(oC), ORP, DO, BOD_5, COD_{total}, $COD_{dissolved}$, total suspended solids (TSS), Total-N, NH_3-N, NO_3-N, NO_2-N, Total-P and PO_4-P measurements were monitored following the Standard Methods 2310, 2320, 2550, 2580, 4500-O, 5210 B, 5220 D, 2540 D, 4500-N, 4500-NH_3, 4500-NO_3, 4500-NO_2 and 4500-P [29]. Inert COD was measured according to glucose comparison method [30]. The samples were analyzed by high pressure liquid chromatography (HPLC) with photodiode array and mass spectrometric detection using an Agilent 1100 high performance liquid chromatography system consisting of an automatic injector, a gradient pump, a Hewlett–Packard series 1100 photodiode array detector, and an Agilent series 1100 VL on-line atmospheric pressure ionization electrospray ionization mass spectrometer to detect polyaromatics namely, 2-methoxy-5-methylaniline, 2,4-diaminoanisole, 4,40-diamino diphenyl-ether, o-aminoazotoluene, 4-aminoazobenzol, respectively. All the metabolites were measured in the same HPLC by mass spectrometric detections. Operation of the system and data analysis were done using ChemStation software, and detection was generally done in the negative ion [M − H]– mode, which gave less complex spectra, although the positive ion mode was sometimes used to reveal fragmentation patterns—especially patterns of sugar attachment.

Measurement of photonic efficiency (lr) of La doped ZnO

The relative photonic efficiency of the catalyst is obtained by comparing the photonic efficiency of La-doped ZnO with that of the standard photocatalyst (ZnO). In order to evaluate l_r, a solution of 1-Methylcyclopropene-MCP (40 mg/L) with a pH of 10 was irradiated with 100 mg of ZnO and La-doped ZnO for 60 min. From the degradation results, Ir was calculated as follows (Eq. 1).

$$I_r = \frac{\textit{initial rate of MCP degradation on La-doped ZnO}}{\textit{initial rate of MCP degradation on pure ZnO}} \quad (1)$$

Operational conditions

Under 10-30-50 and 100 W/L UV light powers the photocatalytic oxidation of the pollutant parameters in the TW at different operational conditions such as at increasing La mass ratios in the La-ZnO nanocomposite (0.5wt% , 1wt%, 1.5wt%, 2wt%), at increasing photooxidation times (5 min, 15 min, 30 min, 60 min, 80 min and 100 min), at different La-ZnO photocatalyst concentrations (1, 5, 15, 30 and 45 mg/L), under acidic, neutral and basic conditions, respectively.

All the experiments were carried out following the batch-wise pro-

cedure. All experiments were carried out three times and the results were given as the means of triplicate sampling with standard deviation (SD) values.

Results and Discussion

XRD Analysis Results

Figure 4 shows the XRD patterns of increasing doped La to ZnO. The nanoparticles recorded in the range of 20–70 degree for different La loadings. The XRD patterns of all the La-doped ZnO catalysts are almost similar to that of ZnO, suggesting that there is no change in the crystal structure upon La loading. In other words, the observed diffraction peaks of the pure ZnO catalyst can be indexed to those of hexagonal wurtzite ZnO (PCPDF79-0207). This also indicates that La^{+3} is uniformly dispersed on ZnO nanoparticles in the form of small La_2O_3 cluster. No special peaks of impurity phases such as Zn or Zn(OH)2 were observed. As can be seen from

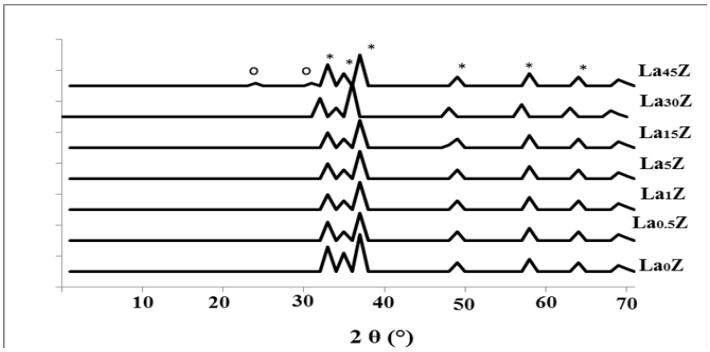

Figure 4: XRD patterns of increasing doped La to ZnO

there is no diffraction peaks originating from lanthanum, and it's compounds in the XRD data up to an addition of 45 mg/l La to La doped ZnO nanocomposite. The absence of La_2O_3 as separate phase might be due to the dissolution of lanthanide in ZnO lattice. From Figure 5, it can be seen that doping of La makes the XRD peak getting wider compared with pure ZnO. To study the effect of doping on the crystallinity of the ZnO nanoparticles, the intensity of the (100), (002), and (101) diffraction peaks was monitored. The intensities of (100), (002), and (101) diffraction peaks were measured as 2200 au, 1700 au, 3004 au, respectively, for 0 mg/l La (Pure nano-ZnO). The intensity of (100), (002) and (101) diffraction peaks decreased from 2200 au to 1350 au; from 1700 au to 100 and from 3004 au to 1305 au in the presence of 1 mg/l La. The maximum diffraction peaks were measured as 1500 au, 1370 au and 1250 au for 30 mg/l La. As the La doped to nano-ZnO ratio increased from 1 mg/l to 30 mg/l the XRD peaks increased and getting wider

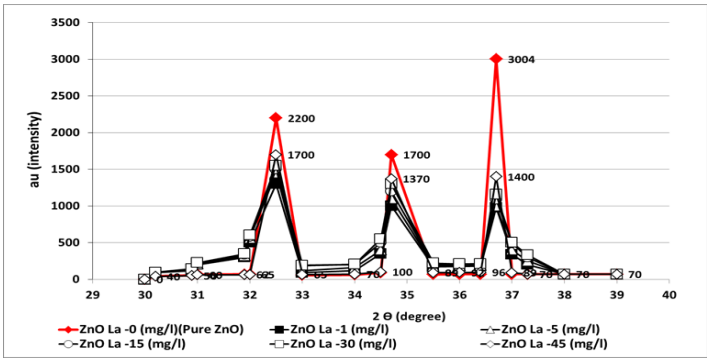

Figure 5: XRD patterns of increasing doped La to ZnO

The width of peak did increased at 45 mg/l La and the intensities of (100), (002) and (101) diffraction peaks were measured as 1700, 1395 and 1490 au. The changes in the peak for crystallinity might be the result of changes in the atomic environment due to impurity doping on ZnO samples as reported by [31].

SEM Analysis Results

The morphology of nanocomposite particles is analyzed by SEM.

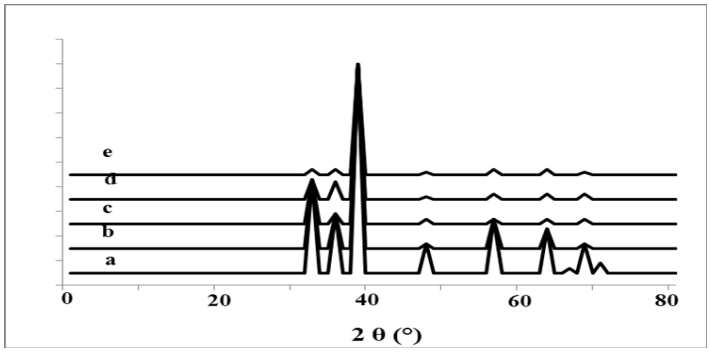

Figure 6: XRD patterns of ZnO and La doped ZnO (a) 2 wt% La doped ZnO (b), (c) 0.5wt% La doped ZnO, (d) 1.0wt% La doped ZnO, and (e) pure ZnO 1.5wt% La doped ZnO.

shows that the nanocomposite material is partly composed of clusters containing composite nanoparticles adhering to each other with a mean size of around 20-80 nm before photooxidation process

while the size was not changed after photooxidation (21-81 nm)

The grains with regular shape are visible and the structure appear porous. The incorporation of lanthanum did not affect the general microstructure and did not significantly affect the grain growth of these materials. This strongly suggests that the ZnO lattice was not severely disrupted by the La ions. The formation of La2O3 can was not observed from the SEM micrograph that shows different morphology clusters not adhered to the grains and it was shown a rough and pore surface.

FTIR Analysis Results

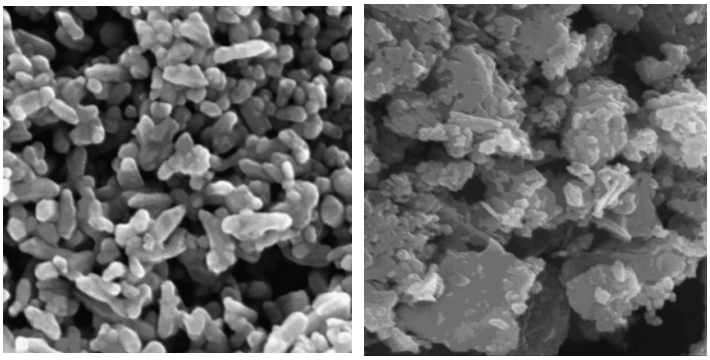

(a) (b)

Figure 7: SEM micrographs of pure and lanthanum modified ZnO, (a) pure ZnO at 25°C, (b) La doped ZnO at 25°C.

shows The FTIR spectrum of 35 mg/l ZnO and 35 mg/l La-doped ZnO concentrations with four different La mass ratios (0.5wt%, 1wt%, 1.5wt% and 2wt%) in the La-doped ZnO nanocomposite. The adsorption bands at 412 and 595 cm-1 are attributed to the Zn-O stretching vibration of wurtzite hexagonal type ZnO crystal, belonging to the oxygen sub-lattice vibration and oxygen vacencies of wurtzite ZnO crystal. The band at 1395 cm-1 is specified as hydrogen-related defects on surface of ZnO. The broad adsorption bands at 3013-3659 cm-1 are the O-H stretching vibration of adsorbed water on ZnO surface.

Adsorption of TW over ZnO and La-doped ZnO

Prior to photocatalytic experiments, adsorption experiments under dark conditions were carried out with 100 ml TW over ZnO and La-doped ZnO catalysts. The TW was stirred on a magnetic stirrer and the aliquots were withdrawn at regular intervals for analysis. There is 2% adsorption of COD over La-doped ZnO whereas it is only 0.5% over ZnO (data not shown). All La-doped ZnO catalysts show sligthly higher adsorption capacities than ZnO. The adsorption of COD in TW is also an important factor for photocatalytic activity.

UV-Visible (UV-Vis) analysis

The UV-Visible absorption spectra of ZnO and La-doped ZnO are shown in Figure 8. The UV-Visible spectra of La-doped ZnOs are shifted to shorter wavelength than that zno alone. as the la doping ıncreased the uv absorbances decreased. The shifting of absorbance maximum towards shorter wavelength was also reported by Liqiang et al (2004). This is attributed to quantum size effects. In addition to quantum size effect, appropriate interaction between surface oxidic site of ZnO and La3+ may also be the cause for shift of wavelength. The absorbance maxima for all the catalysts and the corresponding band gap values and the rate constants for the degradation are presented in Table 1. There is a gradual increase in the bandgap with increase in La loading. Hence the increase in bandgap value with increase in La loading it is quite possible that there is significant interaction between ZnO and La sites.

Effect of increasing La-ZnO nanocomposite concentrations on the removals of TW pollutants

The effects of increasing La-ZnO nanocomposite concentrations (1 mg/L, 5 mg/L, 15 mg/L, 30 mg/L and 45 mg/L), on the photocatalytic oxidation of polutant parameters in the TW was investigated. The preliminary studies showed that the maximum removal of COD with 20 mg/L La-ZnO nanocomposite was 89% with 70 min photooxidation time at pH=7.8 with 40 W UV power (Data not shown). Based on these yields the operational conditions for photocatalytic time were choosen as 60 min at a power of 50 W/L and at a pH of 8. The maximum photocatalytic oxidation removals for all pollutants in the TW were observed at 30 mg/L La-ZnO nanocomposite concentrations, at pH=8.0, after 60 min photooxidation time and at 25°C at a power of 50 W

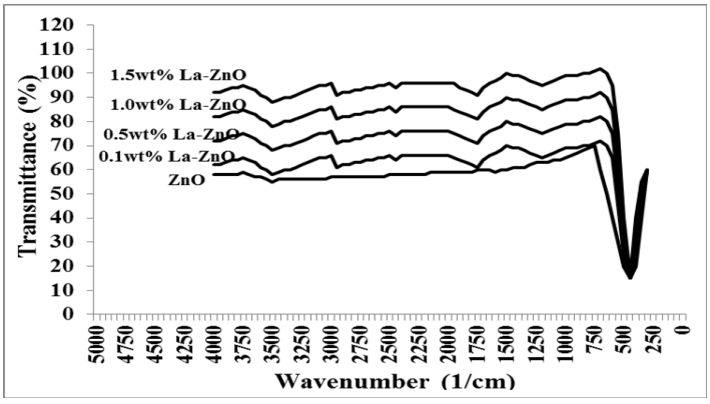

Figure 8: FTIR Spectra of pure ZnO and La-doped ZnO nanoparticles, with different concentration of dopant

Removal efficiencies slightly decreased at 45 mg/L La-ZnO nanocomposite concentration, because over load of surface area of La-ZnO nanocomposites (Figure 6).

This limiting the power of UV irradiation. Lower photo-removal efficiencies was measured for 1, 5, and 15 mg/L La-ZnO concentrations due to low surface areas in the nanocomposite. The surface area is high at 30 mg/L La-ZnO nanocomposite concentrations. Therefore, the maximum photodegradation yield was observed in this nanocomposite concentration. The COD_{total}, COD_{inert}, total flavonols, total aromatic amines and color removals increased as the La-ZnO nanocomposite concentrations were increased from 1 mg/L up to 5 mg/L, to 15 mg/L, and up to 30 mg/L, respectively

Table 2: Effect of increasing La-ZnO nanocomposite concentrations on the TW during photooxidation process after 60 min, at 50 W UV irradiation, at pH=8.0, at 25°C.

Parameters	Removal efficiencies (%)				
	La-ZnO concentrations (mg/L)				
	1 mg/L	5 mg/L	15 mg/L	30 mg/L	45 mg/L
COD_{total}	51	65	84	99	79
COD_{inert}	45	63	78	92	76
$COD_{dissolved}$	50	64	82	98	80
Color	62	69	85	99	83
Total flavonols	40	58	79	91	72
Flavonols					
Kaempferol	35	57	72	87	65
Quercetin	36	61	73	88	67
Patuledin	37	62	79	90	74
Rhamnetin	38	56	72	87	64
Rhamnazin	34	53	71	85	66
TAAs	58	75	81	98	77
Polyaromatics					
2-methoxy-5-methylaniline	55	66	83	93	79
2,4-diaminoanisole	54	71	79	95	73
4,40-diamino diphenyl ether	52	58	68	87	63
o-aminoazotoluene	49	65	75	84	72
4-aminoazobenzol	47	62	76	82	70

Figure 8 Furher increase of nanocomposite concentration to 45 mg/L affect negatively the all the pollutant yields. The reason for this is the optimum amount of catalyst increases the number of active sites on the photocatalyst surface, which in turn increase the number of OH● and superoxide radicals (O_2 - ●) to degrade pollutant parameters (COD components, flavonols, polyaromatics, color). Excess catalyst cause turbidity, prevent the illumination of light, OH●,

Effect of increasing La-ZnO nanocomposite concentrations on the removals of TW pollutants

The effects of increasing La-ZnO nanocomposite concentrations (1 mg/L, 5 mg/L, 15 mg/L, 30 mg/L and 45 mg/L), on the photocatalytic oxidation of polutant parameters in the TW was investigated. The preliminary studies showed that the maximum removal of COD with 20 mg/L La-ZnO nanocomposite was 89% with 70 min photooxidation time at pH=7.8 with 40 W UV power (data not shown). Based on these yields the operational conditions for photocatalytic time were choosen as 60 min at a power of 50 W/L and at a pH of 8. The maximum photocatalytic oxidation removals for all pollutants in the TW were observed at 30 mg/L La-ZnO nanocomposite concentrations, at pH=8.0, after 60 min photooxidation time and at 25°C at a power of 50 W

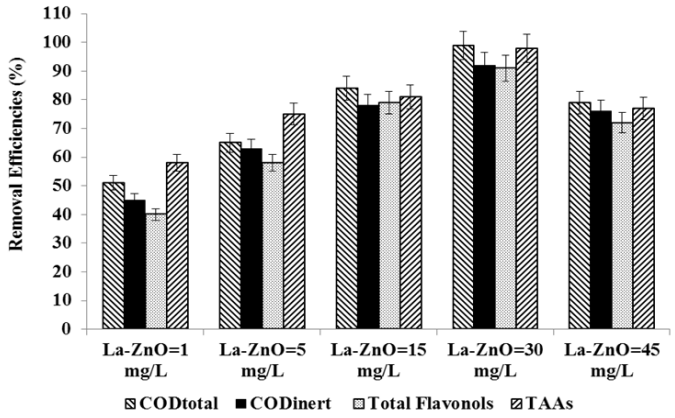

Figure 9: Removal efficiencies of COD_{total}, COD_{inert}, total flavonols and TAAs at La-ZnO=1 mg/L, La-ZnO=5 mg/L, La-ZnO=15 mg/L and La-ZnO=30 mg/L

Removal efficiencies slightly decreased at 45 mg/L La-ZnO nanocomposite concentration, because over load of surface area of La-ZnO nanocomposites (Figure 9). This limiting the power of UV irradiation. Lower photo-removal efficiencies was measured for 1, 5, and 15 mg/L La-ZnO concentrations due to low surface areas in the nanocomposite. The surface area is high at 30 mg/L La-ZnO nanocomposite concentrations. Therefore, the maximum photo-

degradation yield was observed in this nanocomposite concentration. The COD_{total}, COD_{inert}, total flavonols, total aromatic amines and color removals increased as the La-ZnO nanocomposite concentrations were increased from 1 mg/L up to 5 mg/L, to 15 mg/L, and up to 30 mg/L, respectively (Table 2 and Figure 9).

Furher increase of nanocomposite concentration to 45 mg/L affect negatively the all the pollutant yields. The reason for this is the optimum amount of catalyst increases the number of active sites on the photocatalyst surface, which in turn increase the number of OH● and superoxide radicals (O_2 - ●) to degrade pollutant parameters (COD components, flavonols, polyaromatics, color). Excess catalyst cause turbidity, prevent the illumination of light, OH●, a primary oxidant in the photocatalytic system decreased and the efficiency of the degradation reduced accordingly. Furthermore, the increase in catalyst concentration beyond the optimum may result in the agglomeration of catalyst particles; hence, a part of the catalyst surface becomes unavailable for photon absorption, and thereby, photocatalytic oxidation efficiency decreases [32]. Maximum COD_{total}, COD_{inert}, total flavonols, TAAs and color removal efficiencies were obtained after 60 min photooxidation process with yields > 92% at the same operational conditions mentioned above (Figure 9).

Flavonols such as kaempferol, quercetin, patuledin, rhamnetin, rhamnazin removal efficiencies also were >85%, at the same operational conditions (Table 2). Polyaromatic amines such as, 2-methoxy-5-methylaniline, 2,4-diaminoanisole, 4,40-diamino diphenyl ether, o-aminoazotoluene, 4-aminoazobenzol removal efficiencies after photooxidation process varied between 82% and 95% (Table 2). The benzene bounds were cleaved and the -OH and -CH3 groups were separated from the kaempferol under UV irradiation. Kaempferol metabolites such as, 3-O-[2-O, 6-O-bis (α-L- rhamnosyl)-(*ß*-D-glucosyl] quercetin, 3-O-[6-O-(α-L -rhamnosyl)-(*ß*-D - glucosyl] quercetin, 3-O-{2-O-[6-O-(p-hydroxy-*trans*-cinnamoyl)-{)-, *ß*-D -glucosyl]- *á-L-* rhamnosyl} decreased with yields varying between 80% and 85%

Table 3: The metabolites of flavonols in the TW

Flavonoids	Flavonoids metabolites	Influent concentrations (mg/L)	Effluent Concentrations (mg/L)	Removal efficiencies (%)
Kaempferol	3-O-[2-O, 6-O-bis (α-L- rhamnosyl)-(ß-D-glucosyl]-quercetin	5.7	0.86	85
	3-O-[6-O-(α-L -rhamnosyl)-(*ß*-D - glucosyl] quercetin	3.6	0.08	81
	3-O-{2-O-[6-O-(p-hydroxy-trans-cinnamoyl)-{)-, *ß*-D -glucosyl]- *á-L-* rhamnosyl} kaempferol	4.7	0.95	78
Quercetin	3-O-[6-O-(α-L -rhamnosyl)-)-(*ß*-D-glucosyl] quercetin	9.2	1.28	86
	3-O-{2-O-[6-O-(p-hydroxy-trans-cinnamoyl)-(*ß*-D -glucosyl]-- *á-L-* rhamnosyl} quercetin	7.4	1.30	85
Patuledin	(E)-ascladiol	10.3	1.55	85
	(Z)-ascladiol	8.1	0.85	88
Rhamnetin	Methyl quercetin	7.2	1.15	84
	Tetrahydroxy-7-methoxyflavone	4.6	0.44	86
Rhamnazin	Rham nazin-3-0-*ß*-D -glucopyranosyl-(l →5)-*α-L-* arabinofuranoside	6.15	1.42	77
	Rhamnazin-3-O-*ß*-D- glucopyranosyl-(l—»5)-[ß-D-apiofuranosyl-(-1→2)]-*α -L*-arabinofuranoside	5.15	1.05	82

Quercetin metabolites also namely 3-O-[6-O-(α-L -rhamnosyl)-)-(ß-D-glucosyl] quercetin, 3-O-{2-O-[6-O-(p-hydroxy-*trans*-cinnamoyl)-(*ß-D* -glucosyl]-- á-L- rhamnosyl} decreased with high yields (80-89%) under UV (Table 3). Patuledin metabolites such as, (E)-ascladiol, (Z)-ascladiol removed with high yields (80-86%) (Table 3). Rhamnetin metabolites such as, methyl quercetin, tetrahydroxy-7-methoxyflavone removed with high yields (80-87%) under 50 W UV power at 25°C (Table 3). Rhamnazin metabolites such as, Rhamnazin-3-0-ß-D -glucopyranosyl-(l →5)- α-L-arabinofuranoside, Rhamnazin-3-O-ß-D-glucopyranosyl-(l—»5)-[ß-D-apiofuranosyl-(-1→2)]-α-L-arabinofuranoside reduced from 6.5 mg/L to 1.42 mg/L, from 6.5 mg/L to 1.66 mg/L, respectively, after 60 min photooxidation time, at 50 W UV power and at 25°C (Table 3).

2-methoxy-5-methylaniline metabolite such as, 5-nitro-o-toluidine decreased from 134.6 mg/L to 36.34, after 60 min photooxidation time, at pH=8.0, at 30 mg/L La-ZnO nanocomposite concentration

at 50 W UV power and at 25°C

Table 4: The metabolites of polyaromatic amines in the TW.

Polyaromatic amines	Polyaromatic amines metabolites	Influent concentrations (mg/L)	Effluent Concentrations (mg/L)	Removal efficiencies (%)
2-methoxy-5-methylaniline	5-nitro-o-toluidine	134.6	36.34	87
2,4-diaminoanisole	4-acetylamino-2-aminoanisole	275.8	22.06	92
	2,4-diacetylaminoanisole	200,5	38.61	90
4,40-diamino diphenyl ether	N,NI-diacetyl-4,4I-diaminobenzhydrol	156	28.08	82
	N,NI-diacetyl-4,4 I -diaminophenylmethane	116	40.56	84
o-aminoazotoluene	hydroxy-OAT (I)	293.6	58.72	80
	4′ -hydroxy-OAAT	200	79.27	83
	2′ -hydroxymethyl-3-methyl-4-aminoazobenzene	193.6	85.14	84
	4, 4′-bis(otolylazo)-2, 2′ -dimethylazoxybenzene	203.6	117.44	67
4-aminoazobenzol	Phenylhydroxylamine	158	39.16	78
	Nitrosobenzol	108	34.5	75

2,4-diaminoanisole metabolites such as, 4-acetylamino-2-aminoanisole, 2,4-diacetylaminoanisole; 4,40-diamino diphenyl ether metabolites such as, N,NI-diacetyl-4,4I-diaminobenzhydrol, N,NI-diacetyl-4,4 I –diaminophenylmethane and o-aminoazotoluene metabolites such as, hydroxy-OAT (I), 4′ -hydroxy-OAAT, 2′ -hydroxymethyl-3-methyl-4-aminoazobenzene, 4, 4′-bis(otolylazo)-2, 2′ -dimethylazoxybenzene decreased with removals varying between 67% and 92% after 60 min photooxidation time, at pH=8.0, at 30 mg/L La-ZnO nanocomposite concentration at 50 W UV power and at 25oC (Table 4). 4-aminoazobenzol metabolites such as phenylhydroxylamine and nitrosobenzol also removed (Table 4).

The effect of La^{+3} doping concentration on ZnO for the photocatalytic activity of RhB was also investigated. 9 g/L La^{+3}-doped ZnO with a mass ratio of 2wt% had high photocatalytic efficiency [24]. 68.57% Acid Yellow 29 55% Coomassie Brilliant Blue G250 and 37.27% Acid Green 25 degradations was obtained after 120 min of irradiation in the presence of 0.9% La-doped ZnO, at 500 W UV light irradiation, under atmospheric oxygen, at 25°C, respectively [31]. The color and pollutant yields obtained in our study exhibited higher yields compared to the studies given above with low La-ZnO nanocomposite concentrations. 68.57% Acid Yellow 29 55% Coomassie Brilliant Blue G250 and 37.27% Acid Green 25 degradations was obtained after 120 min of irradiation in the presence of 0.9% La-doped ZnO, at 500 W UV light irradiation, under atmospheric oxygen, at 25oC, respectively [27].

Effect of increasing La mass ratios on 30 mg/L La doped ZnO nanocomposite for photodegradation of TW pollutants

Were researched the effects of different La mass ratios (0.5wt%, 1wt%, 1.5wt% and 2wt%) in 30 mg/L La-ZnO nanocomposite concentrations on the photooxidation yields of all pollutants in the TW during photooxidation experiments. Maximum COD_{total}, COD_{inert}, total flavonols, TAAs and color removal efficiencies were 99%, 92%, 91%, 98% and 99%, respectively, after 60 min photooxidation time, at pH=8.0, at 1.5wt% La mass ratio and at 25°C

Table 5: The metabolites of polyaromatic amines in the TW.

Peak No	RT (min)	UV (λmax) (nm)	[M-H]- (m/z)	MS fragments (ESI)	Identification
		345	447.3, 285.3		kaempferol hexose (1)
17	30.7	265,	755.3, 301.3, 271.4,	609.1, 301.1	Quercetin-3-O-2″-(6″-p-
		315,	255.4		-coumaroyl)glucosylrhamnoside (1)
		355			
18	31.53	255,	755.3, 301.3, 271.4,	609.1, 301.1	Quercetin-3-O-2″-(6″-*p*-
		350	255.4		-coumaroyl)glucosylrhamnoside (1)
19	32.02	265,	747.3, 301.3	multiple	Quercetin-3-O-p-coumaroylgdiglycoside (1)
		345			
20	32.31	265,	739.1, 285.3	593.1, 285.1	3-O-[2-O,6-O-Bis(α-L-rhamnosyl)]-β-D-
		315			-glucosyl]kaempferol (4)
21	32.97	265,	739.1, 300.3, 285.3	593.1, 285.1	3-O-[2-O,6-O-Bis(α-L-rhamnosyl)]-β-D-
		340			-glucosyl]kaempferol (4)
22	33.54	265,	739.2, 301.3, 285.3	593.1, 285.1	3-O-[2-O,6-O-Bis(α-L-rhamnosyl)]-β-D-
		345			-glucosyl]kaempferol (4)
23	34.54	265sh, 315	739.2, 301.3, 285.3	593.1, 285.1	3-O-[2-O,6-O-Bis(α-L-rhamnosyl)]-β-D- -glucosyl]kaempferol (4)
24	34.9		423, 847	423.0, 367.1	Gingkolide B (1)
4	17.4	275	787.2, 641.1, 593.2,	625.1,	Isorhamnetin-3-O-rhamnosylhexoside-7-O-
			478.3, 371.1, 315.3	478.2, 315.2	-glucoside (1, 2)
5	18.76	270	771.2, 625.3, 462.3,	609.2,	Quercetin-3-O-rhamnosylhexoside-7-O-glu- co
			305.2, 299.3	463.1, 301.2	(1)
6	19.69	275	729.2, 595.1, 489.1	multiple	Unknown
7	21.32	275	449.3, 287.3	421.0,	Unknown flavonoid hexoside (3)
			287.1, 259.0		
8	22.82	355	755.1, 301.3	593.2	3-O-[2-O,6-O-Bis(α-L-rhamnosyl)]-β-D- glucosyl]quercetin (4)
9	23.55	355	625.3, 316.3	316.2	3-O-[6-O-(α-L-rhamnosyl)-β-D- -glucosyl]isorhamnetin (4)
0	24.14	265sh, 350	739.2, 285.3	285.2	3-O-[2-O,6-O-Bis(α-L-rhamnosyl)]-β-D- -glucosyl]kaempferol (4)
1	24.5	265sh, 355	479.3, 316.3	316.2	3-O-(β-D-Glucosyl)isorhamnetin (4)

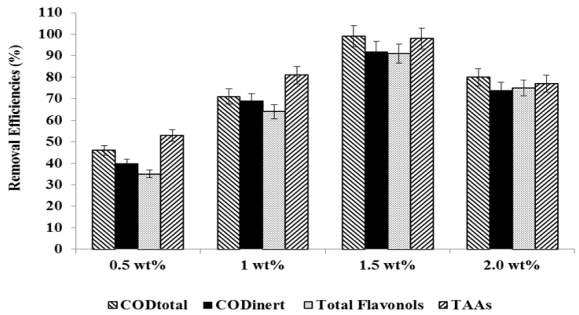

Figure 10: Removal efficiencies of COD_{total}, COD_{inert}, total flavonols and TAAs at 0.5wt%, 1wt%, 1.5wt%, and 2 wt% La mass ratio.

Removal efficiencies increased as the La mass ratio in the La-doped ZnO nanocomposite were increased from 0.5wt% to 1wt% and to 1.5wt%. Maximum removal efficiencies was measured at 1.5wt% La mass ratio in the nanocomposite. The photocatalytic degradation efficiency of ZnO nanoparticles increases with an increase in the La loading and shows a maximum activity at 1.5 wt%. Then decreases in photooxidation yield was observed on further La doping (to 2 wt%). The reason of this can be explained as follows: excessive amounts of dopants can retard the photocatalysis process, because excess amount of dopants deposited on the surface of ZnO increases the recombination rate of free electrons and energized holes, thus inhibiting the photodegradation process. Hence, further increase in La doping to 2wt% results in the decrease of photocatalytic degradation efficiency.

The synthesized La-doped ZnO catalyst possesses smaller particle size distribution than pure ZnO nanoparticles. Apart from their small size, as La^{+3} was doped in ZnO, more surface defects are produced as reported by [33]. Consequently, the migration of the photo-induced electrons and holes toward surface defects is reasonable [33]. Thus, the separation efficiency of the electron–hole pairs of La-doped ZnO with more oxygen defects should be more than that of the pure ZnO nanoparticles. Therefore, the enhancement in the photocatalytic degradation efficiency of La doping ZnO increases due to small particle size and higher defect concentration compared to ZnO alone.

UV absorbances of La-doped ZnO

The UV–vis absorption spectra of ZnO and La-doped ZnO are shown in

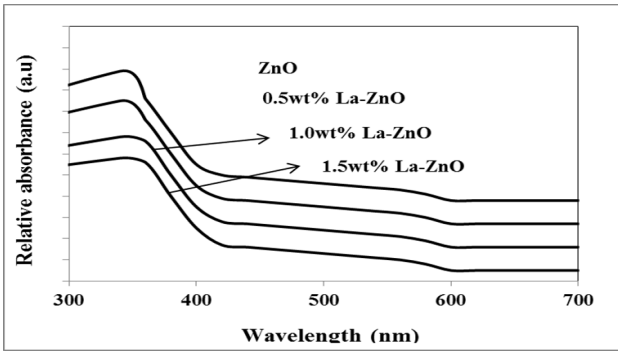

Figure 11: UV-vis absorption spectra of La doped ZnO catalysts

It can be clearly seen from Figure 11. The maximum absorbance shifts is 410 nm for pure nano ZnO while the maximum absorbance of La-doped ZnO with a La mass ratio 0.5wt% is observed at a wavelentgh of 380 nm. The wave of absorbance of La-doped ZnO also increases gradually with increasing the La loading and is much higher as compared to that of pure ZnO. This could be mainly attributed to the quantum size effect as well as the strong interaction between the surface oxides of Zn and La. These observations strongly suggest that the La doping significantly affects the absorbance properties

Table 6. Effect of increasing La mass ratios on the TW during photooxidation process after 60 min, at 50 W UV irradiation, 30 mg/L La-ZnO nanocomposite concentrations, at pH=8.0, at 25°C.

Parameters	Removal efficiencies (%)			
	La mass ratios (%)			
	0.5wt%	1wt%	1.5wt%	2wt%
COD_{total}	46	71	99	80
COD_{inert}	40	69	92	74
$COD_{dissolved}$	45	70	98	78
Color	57	76	99	81
Total flavonols	35	64	91	75
Flavonols				
Kaempferol	30	63	87	68
Quercetin	31	67	88	69
Patuledin	32	68	90	75
Rhamnetin	33	62	87	68
Rhamnazin	30	60	85	67
TAAs	53	81	98	77
Polyaromatics				
2-methoxy-5-methylaniline	50	72	93	69
2,4-diaminoanisole	49	77	95	75
4,40-diamino diphenyl ether	47	64	87	64
o-aminoazotoluene	44	71	84	70
4-aminoazobenzol	41	70	82	66

The strong UV band gap emission (375–395 nm) results from the radiative recombination of an excited electron in the conduction band with the valence band hole. The broad visible or deep-trap state emissions (410–440 nm and 540–580 nm) are commonly defined as the recombination of the electron-hole pair from localized states with energy levels deep in the band gap, resulting in lower energy emission. These deep-trap emissions indicate the presence of defects or oxygen vacancies of ZnO nanostructures [34]. Since the band gap excitation of electrons in ZnO or La-doped ZnO with 254 nm can promote electrons to the conduction band with high kinetic energy, they can reach the solid-liquid interface eas-

ily, suppressing electron–hole recombination in comparison with 365 nm. Hence, the observation of low rate at 254 nm is therefore unexpected [35]. The UV band gap emission of La-doped ZnO nanostructures was increased between 380 and 410 nm after the photocatalytic process of pollutant parameters. The results show that 1.5 wt% La-doped ZnO has maximum activity as compared to other photocatalysts.

Effect of increasing photooxidation time on the photooxidation yields of pollutants in the TW

Six different photooxidation times (5 min, 15 min, 30 min, 60 min, 80 min and 100 min) was examined during photocatalytic oxidation of the pollutants in the TW. To determine the optimum time for maximum removals these pollutant parameters in the TW. The maximum photocatalytic oxidation removals was observed at 60 min photooxidation time, at pH=8.0 using 30 mg/L La doped ZnO with a La mass ratio of 1.5wt% at an UV power of 50 W

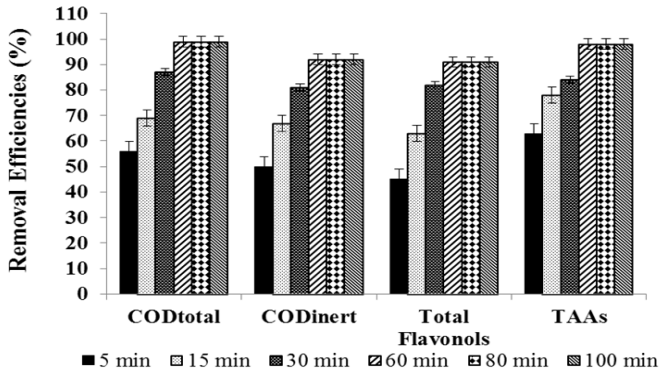

Figure 12: Removal efficiencies of COD_{total}, COD_{inert}, total flavonols and TAAs after 5, 15, 30, 60, 80 and 100 min retention times.

The removals of COD_{total}, COD_{inert}, total flavonols, total aromatic amines and color were found to increase linearly with increase in retention time from 5 min up to 80 min. A further increase in retention time to and 100 min lead to a decrease in yields of pollutant parameters. In other words the removal efficiencies of pollutant parameters (COD components, flavonols, polyaromatics, color) decreased for photooxidation time > 60 min since at long irradiation times since the surface energy of La doped ZnO decreases [36]. The photooxidation can form small molecules such as H2O, carbonmonoxide (CO), CO_2 and benzene etc. after long irradiation; it will lead to the decrease of the polar groups and the oxygen content of pollutant surface. The dispersive component of surface energy, the density of polymer surface has great influence on dispersivity of pollutants in the TW. However, the rate of photodegradation of La doped-ZnO blends increases with the increase of irradiation time, and is higher than that of photocrosslinking after long irradiation time, leading to the decrease of the density of the polymer surface and the dispersivity of COD, dyes and other pollutants to La doped–ZnO[37]. The photooxidation can form small molecules such as H_2O, CO, CO_2 and benzene etc. after long irradiation; it will lead to the decrease of the polar groups and the oxygen content of polymer surface, therefore the dispersivity decreaeses resulting in low photooxidation yields [37]. Aromatic and phenolic metabolites which would adsorb strongly onto titania surface and block significant part of photoreactive sites.

The maximum CODtotal, CODinert, total flavonols, total aromatic amines and color removal efficiencies were 99%, 92%, 91%, 98% and 99%, respectively, after 60 min photooxidation time, at 1.5 wt% La mass ratio in 30 mg/L La-ZnO nanocomposite concentration, at pH=8.0 and at 25°C under 50 W irradiation

Table 7: Effect of increasing photooxidation time on the TW during photooxidation process, at 50 W UV irradiation, at pH=8.0, 30 mg/L La-ZnO nanocomposite concentrations, 1.5 wt% La mass ratio, at 25°C.

Parameters	Removal efficiencies (%)					
	5 min	15 min	530 min	60 min	80 min	100 min
COD_{total}	56	69	87	99	99	99
COD_{inert}	50	67	81	92	92	92
$COD_{dissolved}$	55	68	85	98	98	98
Color	67	74	88	99	99	99
Total flavonols	45	63	82	91	91	91
Flavonols						
Kaempferol	40	61	75	87	86	86
Quercetin	41	65	77	88	86	85
Patuledin	41	66	81	90	89	89
Rhamnetin	43	61	74	87	85	84
Rhamnazin	39	58	72	85	84	84
TAAs	63	78	84	98	98	98
Polyaromatics						

2-methoxy-5-methylaniline	60	71	86	93	93	92
2,4-diaminoanisole	59	75	82	95	94	94
4,40-diamino diphenyl ether	57	62	71	87	79	78
o-aminoazotoluene	55	69	78	84	82	80
4-aminoazobenzol	51	62	75	82	81	79

Also, flavonols such as kaempferol, quercetin, patuledin, rhamnetin, rhamnazin removal efficiencies were 87%, 88%, 90%, 87% and 85%, respectively (Table 7). The photooxidation removals of polyaromatic amines such as, 2-methoxy-5-methylaniline, 2.4-diaminoanisole, 4.40-diamino diphenyl ether, o-aminoazotoluene, 4-aminoazobenzol were 93%, 95%, 87%, 84% and 82%, respectively, after 60 min at pH=8.0 and at 25°C (Table 7). Kaempferol, quercetin, patuledin, rhamnetin, rhamnazin concentrations decreased from 5.7 to 0.741 mg/L, from 9.2 to 1.104 mg/L, from 10.3 to 1.03 mg/L, from 7.2 to 0.936 mg/L, from 6.15 to 0.923 mg/L, respectively. 2-methoxy-5-methylaniline, 2,4-diaminoanisole, 4,40-diamino diphenyl ether, o-aminoazotoluene, 4-aminoazobenzol concentrations decreased from 134.6 to 9.422 mg/L, from 275.8 to 13.79 mg/L, from 156 to 5.46 mg/L, from 293.6 to 10.28, from 178 to 6.23 mg/L, respectively.

The color yields obtained in this study for TW are higher than the studies given below: [27investigated the effects of $Zn_{0.95}La_{0.05}O$ and $Zn_{0.90}La_{0.10}O$ on the treatment of Methylene Blue (MB) dyestuff removal under 18 W UV irradiation for 1 h. 81% color yields were observed for the aforementioned Zn-La-O nanocomposites, respectively [27,28]. found 80% color yields based on Reactive Black 5 after 60 min irradiation time under 90 W irradiation using Zn-Ln nanocomposite.

Effect of increasing UV powers on the yields of pollutants in the TW

In this study, four UV light powers were used (10 W, 30 W, 50 W and 100 W) to detect the optimum UV irradiation power for maximum photo-removal of the pollutant parameters in the TW using 30 mg/L La poped ZnO nanocomposite with a La mass ratio of 1.5%w. The maximum photocatalytic oxidation removals was observed at 50 W UV light irradiation, at pH=8.0, after 30 min photooxidation time and at 25°C

Table 8. Effect of increasing UV light irradiations on the TW during photooxidation process after 60 min, at 30 mg/L La-ZnO photocatalyst concentration, at pH=8.0, at 25°C.

Parameters	Removal efficiencies (%)			
	UV light irradiation			
	10 W	30 W	50 W	100 W
CODtotal	49	82	99	97
CODinert	43	76	92	90
CODdissolved	48	81	98	96
Color	60	83	99	99
Total flavonols	38	76	91	90
Flavonols				
Kaempferol	33	70	87	87
Quercetin	34	71	88	86
Patuledin	35	78	90	89
Rhamnetin	36	70	87	87
Rhamnazin	33	71	85	85
TAAs	56	79	98	96
Polyaromatics				
2-methoxy-5-methylaniline	53	81	93	92
2,4-diaminoanisole	52	77	95	93
4,40-diamino diphenyl ether	50	66	87	86
o-aminoazotoluene	47	73	84	81
4-aminoazobenzol	45	71	82	80

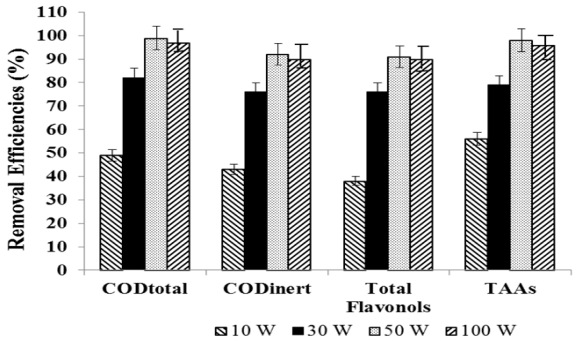

Figure 13: Removal efficiencies of COD_{total}, COD_{inert}, total flavonols and TAAs at 10 W, 30 W, 50 W and at 100 W.

The COD_{total}, COD_{inert} total flavonols, total aromatic amines and color were found to increase linearly with increase in UV light irradiation from 10 W, up to 30 W, up to 50 W, respectively (Table 8 and Figure 13). Further increase of UV power up to 100 W did not affect positively the pollutant yields. Maximum COD_{total}, COD_{inert}, total flavonols, TAAs and color removal efficiencies after photooxidation process were 99%, 92%, 91%, 98% and 99%, respectively, for the aforementioned operational conditions (Figure 13). Flavonols such as kaempferol, quercetin, patuledin, rhamnetin, rhamnazin removal efficiencies were 87%, 88%, 90%, 87% and 85%, respectively, after 60 min photooxidation time, at 50 W UV light, at pH=8.0, at 30 mg/L La-ZnO nanocomposite concentration and at 25oC (Table 8). Polyaromatic amines such as, 2-methoxy-5-methylaniline, 2, 4-diaminoanisole, 4, 40-diamino diphenyl ether, o-aminoazotoluene, 4-aminoazobenzol removal efficiencies after photooxidation process were 93%, 95%, 87%, 84% and 82%, respectively (Table 8).

The UV power determines the extent of light absorption by the semiconductor catalyst at a given wavelength. During initiation of photocatalysis, electron–hole formation in the photochemical reaction is strongly dependent on the optimum light intensity[38]. In this study, as the UV power increase from 10 W up to 50 W might favor a high-level surface defects, which account for the increase in the defect emission relative to the UV emission as reported by [35]. Higher UV powers > 50 W decrease the defects in the surface of the nanoparticle by disturbing the active holes.

Effect of increasing pH values on the pollutant yields in the TW

The effects of increasing pH values (4.0, 6.0, 8.0 and 10.0) on the photocatalytic oxidation of polutant parameters in TW was examined by considering the solubility of ZnO nanoparticles in acidic as well as in highly basic solutions. The maximum photocatalytic oxidation removals was obtained at pH=8.0, after 60 min photooxidation time with a La mass ratio 1.5wt% using 30 mg/L La-ZnO nanocomposite concentration at 50 W UV power

Table 9: Effect of increasing pH values on the TW during photooxidation process, at 50 W UV irradiation, after 60 min, at 25°C

Parameters	Removal efficiencies (%)			
	pH values			
	pH=4.0	pH=6.0	pH=8.0	pH=10.0
COD_{total}	53	74	99	72
COD_{inert}	47	72	92	70
$COD_{dissolved}$	52	73	98	71
Color	64	79	99	77
Total flavonols	42	68	91	66
Flavonols				
Kaempferol	37	66	87	64
Quercetin	38	70	88	68
Patuledin	39	71	90	69
Rhamnetin	40	66	87	64
Rhamnazin	45	62	85	60
TAAs	60	83	98	81
Polyaromatics				
2-methoxy-5-methylaniline	57	76	93	74
2,4-diaminoanisole	56	80	95	78
4,40-diamino diphenyl ether	54	67	87	65
o-aminoazotoluene	52	74	84	72
4-aminoazobenzol	50	65	82	63

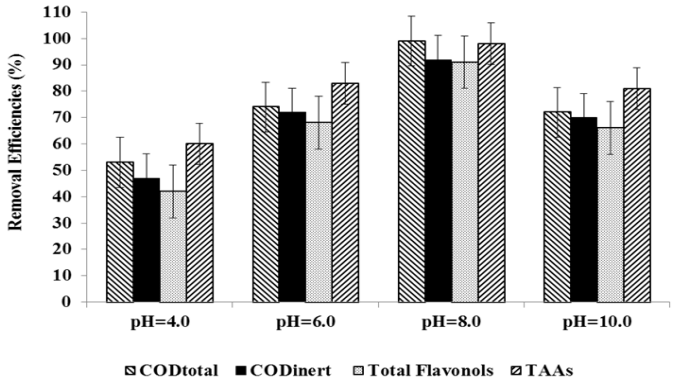

Figure 14: Removal efficiencies of COD_{total}, COD_{inert}, total flavonols and TAAs at pH=4.0, pH=6.0, pH=8.0, pH=10.0

In acidic medium, less photocatalytic degradation of pollutant parameters (COD components, flavonols, polyaromatics, color) was observed. The extent of photocatalytic degradation of polutant parameters was found to increase with increase in initial pH to 8.0 and a decrease in maximum photocatalytic degradation was found at pH 10. The possible explanation of this is that the pH at zero point charge (zpc) of ZnO is 9.0 ± 0.3 [15]. Below pH 8.0, active sites on the positively charged catalyst surface are preferentially covered by pollutant molecules. Thus, surface concentration of the polutant parameters (COD components, flavonols, polyaromatics, color) is relatively high, while those of OH- and OH• are low. Hence, photocatalytic degradation decreases at acidic pH. On the other hand, above pH 8.0, catalyst surface is negatively charged by means of metal-bound OH-, consequently the surface concentration of the polutant parameters (COD components, flavonols, polyaromatics, color) is low, and OH• is high. In addition, polutant parameters are not protonated above pH 8.0. The electrostatic repulsion between the surface charges and La doped ZnO nanocomposite hinders the amount of polutant parameters and the adsorption, consequently surface concentration of the polutant parameters decreases, which results in the decrease of photocatalytic degradation at pH 10.0. In conclusion, pH 8.0 can provide moderate surface concentration of polutant parameters which react with the holes to form OH•.

Photocatalytic oxidation mechanisms of La doped ZnO nanocomposite

The higher activity of La doped ZnO can be attributed to successful e−–h+ separation and production of •O_2− and OH•. La-modified ZnO sample manifests the highest efficiency, which may be explained by the highest number of O_2 vacancies (related to the different charge and electronegativity of La and Zn ions) and as a result of stronger adsorption of OH−ions onto the ZnO surface [18]. This favors the formation of OH• by reaction of hole and OH−. The OH• and photogenerated •O2− has extremely strong non-selective oxidants lead to the degradation of the organic pollutant at the surface of La modified ZnO [37]. The photocatalytic degradation mechanism starts with the illumination of ZnO nanoparticles and production of electron–hole pairs in Eq. (2):

$$ZnO + h_v(UV) \rightarrow e^- + h^+ \quad (2)$$

Major roles of metal ions in this study are to increase the concentration of ZnO on the surface of the catalyst and to prolong the individual life-time of electrons and holes and hence, inhibit their recombination. The ability of La^{+3} to scavenge photogenerated electrons is as follows: (Eq. 3):

$$La^{+3} + e^- \rightarrow La^{+2} \quad (3)$$

However, stabilities of La^{+3} ions may be disturbed in their reduced forms (La^{+2}). This can be achieved by transferring the trapped electron to O_2 [Eq. (4)]:

$$La^{+2} + O_2 \rightarrow La^{+3} + O_2^{-\bullet} \quad (4)$$

The produced $O_2^{-\bullet}$ is responsible from the generation of OH•, known as highly reactive electrophilic oxidants [Eqs. (5-7)]:

$$O_2^{-\bullet} + H^+ \rightarrow HO_2^{\bullet} \quad (5)$$

$$2HO_2^{\bullet} \rightarrow H_2O_2 + O_2 \quad (6)$$

$$H_2O_2 + e^- \rightarrow OH^- + OH^{\bullet} \quad (7)$$

In the meantime, photogenerated holes may react with H_2O molecules and produce OH• (Eq. 8):

$$h^+_{VB} + H_2O \rightarrow H^+ + OH^{\bullet} \quad (8)$$

The color removal by photooxidation of dyes reactions were given in Eqs (9-14):

$$Dye + h_v \rightarrow Dye^* \quad (9)$$

$$Dye^* + La\,doped\,ZnO \rightarrow Dye^+ + La - ZnO(e) \quad (10)$$

$$La - ZnO(e) + O_2 \rightarrow LaO - ZnO + O_2 \quad (11)$$

$$O_2^{-\bullet} + La - ZnO(e) \rightarrow 2H^+ + H_2O_2 \quad (12)$$

$$H_2O_2 + La - ZnO(e) \rightarrow OH^{\bullet} + OH^- \quad (13)$$

$$Dye^+ + O_2\ (or\ O_2^{-\bullet}\ or\ OH^{\bullet}) \rightarrow peroxylated\ or\ hydroxylated\ intermediates \rightarrow degraded\ or\ mineralized\ products \quad (14)$$

Thus, loading of metal ions such as La on the surface of ZnO matrix can suppress the recombination of photoinduced charge carriers either with only electron capture ability or with steps forward to produce OH•. For La–ZnO, electron accepting ability, production of more OH•, the highest surface roughness value and the higher dark adsorption capacity result in pronounced photoactivity. The decay profile of the products includes the subsequent attacks of OH•, known as highly reactive electrophilic oxidants. The main reaction pathway (60% of OH•) is the addition of the OH• to the double bond of the azo group, resulting in the rapid disappearance of color; however, addition to the aromatic ring also occurs (40% of OH•) [39,40]. Further OH• attacks and the increment in OH• concentration in the solution increase the yield of OH-adduct in the degradation progress of each product. The opening of the dye aromatic rings due to consecutive oxidation reactions leads to low-molecular weight compounds [41].

It is concluded that the optimum loading of La^{3+}, Nd^{3+} and Sm^{3+} is 4, 4 and 8 mol%, which may be more efficient for separating photoinduced electron–hole pairs and enhance the photocatalytic activity. The reason for the high activity of Ln-doped ZnO on the photocatalytic activity can be explained by the following mechanism. Under the irradiation lanthanides ions work as an electron

scavenger, that may react with the superoxide species and prevent the holes–electrons (h+/e−) recombination, and thus increases photooxidation efficiency. The possible reaction is represented as follows. Direct band gap excitation of the semiconductor results in electron–hole separation. The high oxidative potential of the hole (hVB+) in the catalyst permits the direct oxidation of organic matter (4-NPh) to reactive intermediates. Very reactive hydroxyl radicals can also be formed either by the decomposition of water or by the reaction of the hole with OH−, as described in the following equations. The hydroxyl radical and photo generated holes are an extremely strong, non-selective oxidants that lead to degradation of the 4-NP at the catalysts surface [35]. (Eq. 15, Eq. 16, Eq. 17 and Eq. 18)-:

$$ZnO + h^+ \rightarrow ZnO\,(eCB^- + hVB^+) \quad (15)$$

$$hVB^+ + 4-NPh \rightarrow oxidation\ of\ 4-NPh \quad (16)$$

$$hVB^+ + H_2O \rightarrow H^+ + OH^\bullet \quad (17)$$

$$hVB^+ + OH \rightarrow OH^\bullet \quad (18)$$

Electron in the conduction band (eCB−) on the catalyst surface can reduce molecular oxygen to superoxide anion (Eq. (20)). This radical, in the presence of organic scavengers, may form organic peroxides (Eq. (21)) or hydrogen peroxide (Eq. (22)):

$$Ln^{+3} + O_2 \rightarrow Ln^{+2} + O_2 \quad (19)$$

$$eCB^- \rightarrow O_2 \rightarrow O_2^{-\bullet} \quad (20)$$

$$O_2^{-\bullet} + 4-NPh \rightarrow 4-NPhOO^\bullet \quad (21)$$

$$O2^{-\bullet} + HO_2^\bullet + H^+ \rightarrow H_2O_2 + O_2 \quad (22)$$

Electrons in the conduction band are also responsible for the production of hydroxyl radicals, which have been indicated as the primary cause of organic matter mineralization (Eq. (23) [35].

$$OH^\bullet + 4-NPh \rightarrow degradation\ of\ 4-NPh \quad (23)$$

The hydroxyl radical and photogenerated holes are an extremely strong, non-selective oxidants that lead to degradation of the 4-NP at the catalysts surface [35]. The TOC, IC and TC concentration values for Nd_4Z (the best photocatalyst in our work) were prove that high mineralization of 4-NPh was achieved. Before catalytic reaction, TOC, IC and TC were 15.4, 0 and 15.4, after 195 min the TC, IC and TOC were 2.9, 2.7 and 0.3, respectively, so mineralization has been occurred and only a few amount of organic carbon was remained. With the increase in Ln+3 ion concentration, the surface barrier becomes higher, the space charge region becomes narrower, and hence the electron–hole pairs are efficiently separated by the large electric field. On the other hand, with the increase in concentration of Ln^{+3} ions, the penetration depth of light into ZnO can greatly exceed the space charge layer. Therefore, the recombination of photogenerated electron–hole pairs becomes easier, which led to a lower photocatalytic activity of ZnO for 4-NP degradation. Therefore, an optimum concentration of Ln+3 ions is required to match the thickness of charge layer and the depth of the light penetration for separating photoinduced electron–hole pairs. In addition, appropriate loading of Ln^{+3} ions is highly necessary for producing a significant potential difference between the surface and the center of the particles in order to efficiently separate the photoinduced electron–hole pairs, because the excess Ln_2O_3 covering the surface of ZnO may increase the number of recombination centers, thus, giving low photocatalytic activity. This can be clearly seen from the present study that Ln-doped ZnO with more than 4, 4 and 8 mol% of La, Nd and Sm loadings showed a low photocatalytic activity. The higher activity of them can be attributed to a strong absorption of OH− ions on the surface of ZnO because of a large number of oxygen vacancies. These OH− ions are assumed to serve as surface-bound traps for the photogenerated holes which prevent electron–hole recombination[36].

The reproducibility of the best catalyst (Nd_4Z), in our work, for 4-NP photodegradation in a three-cycle experiment is performed. After each degradation experiment, to avoid catalyst (4 mol%Nd-doped ZnO) lost, the solution was evaporated at 80oC, and then 100 mL 4-NP solution (10 ppm) was affiliated in 250 mL beakers. 83.43% of 4-NP could be degraded when Nd/ZnO was used for the first time, however, after three recycles, there was not a significant decrease for photocatalytic activity of Nd/ZnO and 81.63% of 4-NP was degraded within 195 min. Doping of Ln cations can provide a more efficient charge separation, increased lifetime of charge carriers and enhanced interfacial charge transfer to absorbed substrates. The repeatability of 4-NP degradation indicates that it is indeed a photocatalytic reaction.

Photonic efficiency of La doped ZnO

In order to evaluate the relative photonic efficiency (Ir), a solution of MCP (40 mg/L) adjusted to pH 10 was irradiated with 100 mg ZnO (Merck) and La-doped ZnO, separately. The relative photonic efficiencies of light of wavelengths 254 and 365 nm for ZnO and La-doped ZnO are presented in

Table 10: Comparison of relative photonic efficiencies in the photodegradation of pollutants in TW by ZnO and La-doped ZnO photocatalysts (*)

Parameters	Relative photonic efficiency (I_r)	
	256 nm	370 nm
Pure ZnO	1.01 ± 0.001	0.79 ± 0.01
0.1wt% La–ZnO	1.09 ± 0.01	0.93 ± 0.01
0.5 wt% La–ZnO	1.28 ± 0.02	0.94 ± 0.01
1.0wt% La–ZnO	2.59 ± 0.01	2.22 ± 0.01
1.5wt% La–ZnO	2.98 ± 0.01	2.25 ± 0.01
2wt% La–ZnO	1.02± 0.01	1.98 ± 0.01
Commercial ZnO	1.02 ± 0.01	1.02 ± 0.01
TiO_2	1.38 ± 0.01	1.03 ± 0.01

(*): pH 5; UV = 8 lamps; ë = 254 and 365 nm; 50 W UV power, 60 min photooxidation time

For comparison, the relative photonic efficiency of TiO2 is also presented in Table 10. The relative photonic efficiencies of La-doped ZnO are greater as compared to those of ZnO and TiO2, revealing the effectiveness of metal-doped systems. It is also interesting to note that the relative photonic efficiency for La-doped ZnO for light of wavelength 254 nm are much higher as compared to that for 365 nm. The results are in good agreement with degradation and mineralization studies. Comparing the high efficiency of La doped ZnO catalysts with standard ZnO and TiO2 catalyst, the photocatalytic efficiency of 1.5 wt% La-doped ZnO is higher as compared to that of ZnO and TiO2 and other La doped ZnO nanocomposites.

UV-Visible (UV-Vis) analysis

The UV-visible absorption spectra of ZnO and La-doped ZnO are shown in

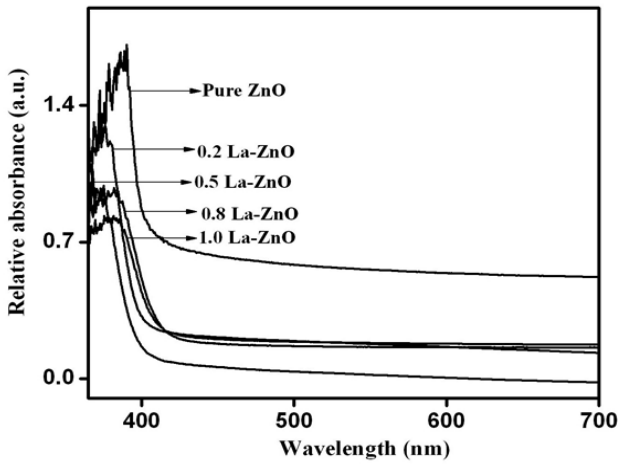

Figure 15: The UV-visible absorption spectra of ZnO and La-doped ZnO

The UV-visible spectra of La-doped ZnOs are shifted to shorter wavelength than that ZnO alone. As the La doping increased the UV absorbances decreased. The shifting of absorbance maximum towards shorter wavelength was also reported by [24]. This is attributed to quantum size effects. In addition to quantum size effect, appropriate interaction between surface oxidic site of ZnO and La^{+3} may also be the cause for shift of wavelength. The absorbance maxima for all the catalysts and the corresponding band gap values and the rate constants for the degradation of kaempferol and 2-methoxy-5-methylaniline are presented in

Table 11: UV-Vis absorption data for ZnO and La-doped ZnO catalysts

Nanomaterial	λmax (nm)	Band gap (eV)	Photodegradation rate constant k (x 10^{-2} min^{-1})
			Polyaromatic amines (for 2-methoxy-5-methylaniline)
ZnO	390	3.80	2.24
0.5 wt% La-ZnO	376	3.30	4.78
1 wt % La-ZnO	375	3.31	5.99
1.5 wt% La-ZnO	374	3.32	7.21
2.0 wt % La-ZnO	369	3.37	2.21

There is a gradual increase in the bandgap with increase in La loading. Hence the increase in bandgap value with increase in La loading it is quite possible that there is significant interaction between ZnO and La sites.

Effect of increasing La-ZnO nanocomposite concentrations on the removals of TW pollutants

The effects of increasing La-ZnO nanocomposite concentrations (1 mg/L, 5 mg/L, 15 mg/L, 30 mg/L and 45 mg/L), on the photocatalytic oxidation of polutant parameters in the TW was investigated. The preliminary studies showed that the maximum removal of COD with 20 mg/L La-ZnO nanocomposite was 89% with 70 min photooxidation time at pH=7.8 with 40 W UV power (data not shown). Based on these yields the operational conditions for photocatalytic time were choosen as 60 min at a power of 50 W/L and at a pH of 8. The maximum photocatalytic oxidation removals for all pollutants in the TW were observed at 30 mg/L La-ZnO nanocomposite concentrations, at pH=8.0, after 60 min photooxidation time and at 25°C at a power of 50 W (Figure 9). Removal efficiencies slightly decreased at 45 mg/L La-ZnO nanocomposite concentration, because over load of surface area of La-ZnO nanocomposites (Figure 9).

This limiting the power of UV irradiation. Lower photo-removal efficiencies was measured for 1, 5, and 15 mg/L La-ZnO concentrations due to low surface areas in the nanocomposite. The surface area is high at 30 mg/L La-ZnO nanocomposite concentrations. Therefore, the maximum photodegradation yield was observed in this nanocomposite concentration. The COD_{total}, COD_{inert}, total flavonols, total aromatic amines and color removals increased as

the La-ZnO nanocomposite concentrations were increased from 1 mg/L up to 5 mg/L, to 15 mg/L, and up to 30 mg/L, respectively (Table 2 and Figure 9). Furher increase of nanocomposite concentration to 45 mg/L affect negatively the all the pollutant yields. The reason for this is the optimum amount of catalyst increases the number of active sites on the photocatalyst surface, which in turn increase the number of $OH^{\bullet}$ and superoxide radicals ($O_2^{\bullet -}$) to degrade pollutant parameters (COD components, flavonols, polyaromatics, color). Excess catalyst cause turbidity, prevent the illumination of light, $OH^{\bullet}$.

Reusability of La doped ZnO

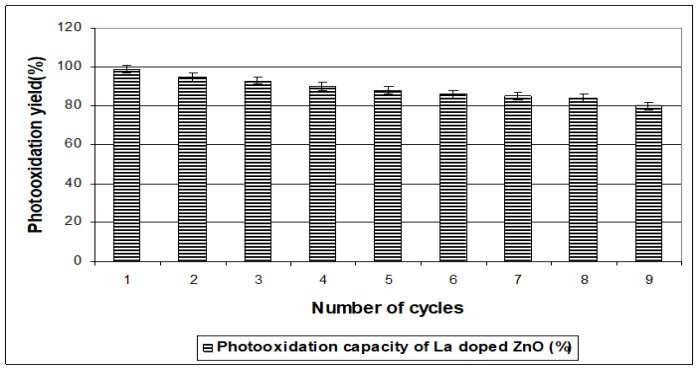

Figure 16. The reusability of La doped ZnO

After the first cycle of photocatalytic oxidation within 60 min, 99% of the La doped ZnO with a mass ratio of 1.5wt% was recovered. After three cycles, the phoooxidation ability of La doped ZnO nanocomposite was retained at 93% of the original value. After 8th cycles the nanocomposite was reatined at 80%. One of the reasons for the slight decline in photooxidation is that the surface of the reused photocatalysts may exist with some low residual substances which did not occupy the photocatalytic sites and did not block the adsorption. The presence of La significantly changed the binding site of the pollutant molecules. It is possible that the oxygen atom in La-ZnO was bound to the dopant La [42]. The speedily recovering of the photodegradation capacity of La doped ZnO for pollutans photodegradation will benefit to their photocatalytic activity.

Conclusions

Hence excess La_2O_3 covering the surface of ZnO can increase the number of recombination centers, thus giving low photocatalytic activity. La loading greater than 0.8 wt% in the present study does not show high photocatalytic activity. By using 30 mg/L La-ZnO with a La mass ratio of 1.5w% the COD_{total}, COD_{inert}, flavonols, polyaromatics and color were photodegraded with yields as high as 82-99% within 60 min photooxidation time, at 25°C under 50 W UV power, at pH=8.0. The addition of La to ZnO lead to enhance the photocatalytic activity by increasing the total surface area. The flavonoids and polyaromatic amines and their metabolites in the TW were firstly determined photodegraded with high rates and photonic efficiency using 30 mg/L La-ZnO with a La mass ratio of 1.5w% at pH 8.

Acknowledgements

This research study was undertaken in the Environmental Microbiology Laboratory at Dokuz Eylül University Engineering Faculty Environmental Engineering Department, İzmir, Turkey. The authors would like to thank this body for providing financial support.

References

1. Lin S H, Chen M L (1997) Treatment of textile wastewater by chemical methods for reuse. Water Research, 31: 868-876.
2. F P van der Zee, R H Bouwman, D P Strik, G Lettinga, J A Field, et al. (2001) Application of redox mediators to accelerate the transformation of reactive azo dyes in anaerobic bioreactors. Biotechnology and Bioengineering, 75:691-701.
3. Chung K T, Stevens S E J (1993) Degradation of azo dyes by environmental microorganisms and helminthes. Environmental Toxicology and Chemistry, 12: 2121-2132.
4. Weisburger J H (2002) Comments on the history and importance of aromatic and heterocyclic amines in public health. Mutation Research: Fundamental and Molecular Mechanisms of Mutagenesis, 506: 9-20.
5. Oliveira D P, Carneiro P A, Sakagami M K, Zanoni M V B, Umbuzeiro G A, et al. (2007) Chemical characterization of a dye processing plant effluent–identification of the mutagenic components. Mutation Research: Fundamental and Molecular Mechanisms of Mutagenesis, 626: 135-142.
6. Robinson T, McMullan G, Marchant R, Nigam P (2001) Remediation of dyes in textile effluent: a critical review on current treatment technologies with a proposed alternative. Bioresource Technology, 77: 247-255.
7. Van der Zee F P, Villaverde S (2005) Combined anaerobic aerobic treatment of azo dyes—a short review of bioreactor studies. Water Research, 39: 1425-1440.
8. Roosta M, Ghaedi M, Shokri N, Daneshfar A, Sahraei R, et al. (2014) Experimental design based response surface methodology optimization of ultrasonic assisted adsorption of safaranin o by tin sulfide nanoparticle loaded on activated carbon. Spectrochimica Acta, Part A: Molecular and Biomolecular Spectroscopy, 122: 223-231.
9. Tavakkoli H, Moayedipour T (2014) Fabrication of perovskite-type oxide La0.5Pb0.5MnO3 nanoparticles and its dye removal performance. Journal of Nanostructure in Chemistry, 4:116-124.
10. Bard A J (1980) Photoelectrochemistry. Science, 207: 139-144.
11. Law M, Greene L E, Johnson J C, Saykally R, Yang P D, et al. (2005) Nanowire dye-sensitized solar cells. Nature Materials, 4: 455-459.
12. Li L, Pan S S, Dou X C, Zhu Y G, Huang X H, et al. (2007) Direct electrodeposition of ZnO nanotube arrays in anodic alumina membranes. Journal of Physical Chemistry C, 111:7288-7291.
13. Marci G, Augugliaro V, Munoz M J L, Martin C, Palmisano L, et al. (2001) Preparation, characterisation and photocatalytic activity of polycrystalline ZnO/TiO2 systems. part 1. surface, bulk characterisation and 4-nitrophenol photodegradation in liquid-solid regime, 105:1033-1040.
14. Khodja A A, Sehili T , Pitichowshi J F, Boule P (2001) Photocatalytic degradation of 2-phenylphenol on TiO2 and ZnO in aqueous suspensions. Journal of Photochemistry and Photobiology A, 141: 231-239.
15. Anandan S, Vinu A, Venkatachalam N, Arabindoo B, Muru-

gesan V,et al. (2006) Photocatalytic activity of ZnO impregnated Hâ and mechanical mix of ZnO/Hâ in the degradation of monocrotophos in aqueous solution. Journal of Molecular Catalysis A: Chemical, 256:312-320.
16. Gouvea K, Wypych F, Moraes S G, Duran N, Nagata N, et al. (2000) Semiconductor-Assisted photocatalytic degradation of reactive dyes in aqueous solution. Chemosphere, 40:433-440.
17. Pareek V K, Adesina A A (2003) Handbook of Photochemistry and Photobiology, ed. By Nalwa HS, American Scientific Publishers, Stevenson Ranch, CA, 1: 345-412.
18. Anandan S, Vinu A, Mori T, Gokulakrishnan N, Srinivasu P, et al. (2007).Photocatalytic degradation of 2,4,6-trichlorophenol using lanthanum doped ZnO in aqueous suspension. Catalysis Communications, 8: 1377-1382.
19. Senthilvelan S, Chandraboss V L, Karthikeyan B, Murugavelu M, Loganathan B, et al. (2012) Novel sol-gel synthesis of cerium-doped ZnO thin films for photocatalytic activity. AIP Conference Proceedings, 1461: 395-398.
20. Hsiao K C, Liao S C, Chen Y J (2007) Synthesis, characterization and photocatalytic property of nanostructured Al-doped ZnO powders prepared by spray pyrolysis. Materials Science and Engineering A, 447: 71-76.
21. Wu C, Shen L, Zhang Y C, Huang Q (2011) Solvothermal synthesis of Cr-doped ZnO nanowires with visible light-driven photocatalytic activity. Materials Letters, 65, 1794-1796.
22. Ganesh I, Sekhar P S C, Padmanabham G, Sundararajan G (2012) Influence of Li-doping on structural characteristics and photocatalytic activity of ZnO nano-powder formed in a novel solution pyro-hydrolysis route. Applied Surface Science, 259, 524-537.
23. Anandan S, Vinu A, Sheeja Lovely, Gokulakrishnan N, Srinivasu P, et al. (2007) Photocatalytic activity of La-doped ZnO for the degradation of monocrotophos in aqueous suspension. Journal of Molecular Catalysis A: Chemical, 266: 149-157.
24. Jia T, Wang W, Long F, Fu Z, Wang H, et al. (2009) Fabrication, characterization and photocatalytic activity of La-doped ZnO nanowires. Journal of Alloys and Compounds, 484: 410-415.
25. Byrappa K, Subramania A K, Ananda S, Rai K M L, Dinesh R, et al. (2006) Photocatalytic degradation of Rhodamine B dye by ZnO. Bulletin of Material Science, 29: 433-438.
26. Sobana N, Swaminathan M (2007) The effect of operational parameters on the photocatalytic degradation of Acid Red 18 by ZnO. Separation and Purification Technology, 56:101-107.
27. Suwanboon S, Amornpitoksuk P, Bangrak P, Muensit N (2013) Optical, photocatalytic and bactericidal properties of Zn1-xLaxO and Zn1-xMgxO nanostructures prepared by a sol–gel method. Ceramics International, 39: 5597-5608.
28. Kaneva N, Bojinova A, Papazova K, Dimitrov D (2015). Photocatalytic purification of dye contaminated sea water by lanthanide (La3+, Ce3+, Eu3+) modified ZnO. Catalysis Today, 252: 113-119.
29. Eaton A D, Clesceri L S, Rice E W, Greenberg A E, Franson M A H, et al. (2005) Standard Methods for the Examination of Water and Wastewater, Ed. by Franson MAH, (21th ed.) American Public Health Association (APHA), American Water Works Association (AWWA), Water Environment Federation (WEF), American Public Health Association (APHA) 800 I Street, NW, Washington, DC USA, 20001-3770: (2005).
30. Germirli F, Orhon D, Artan N (1991) Assessment of the initial inert soluble COD in industrial wastewater. Water Science and Technology, 23:1077-1086.
31. Raza W, Haque M M, Muneer M (2014) Synthesis of visible light driven ZnO: characterization and photocatalytic performance. Applied Surface Science, 322: 215-224.
32. Huang M, Xu C, Wu Z, Huang Y, Lin J, et al. (2008) Photocatalytic discolorization of Methyl Orange solution by Pt modified TiO2 loaded on natural zeolite. Dyes Pigments, 77: 327-334.
33. Zheng Y, Chen C, Zhan Y, Lin X, Zheng Q, et al. (2007) Luminescence and photocatalytic activity of ZnO nanocrystals: correlation between structure and property. Inorganic Chemistry, 46: 6675-6682.
34. Bohle D S, Spina C J (2009) Cationic and anionic surface binding sites on nanocrystalline zinc oxide: surface influence on photoluminescence and photocatalysis. Journal of the American Chemical Society, 131: 4397-4404.
35. Selvam N C S, Vijaya J J, Kennedy L J (2013) Comparative studies on influence of morphology and La doping on structural, optical, and photocatalytic properties of zinc oxide nanostructures. Journal of Colloid and Interface Science, 407: 215-224.
36. Fox M A, Dulay M T (1993) Hetereogeneous photocatalysis. Chemical Reviews, 93: 341-357.
37. Korake P V, Dhabbe R S, Kadam A N, Gaikwad Y B, Garadkar K M, et al. (2014) Highly active lanthanum doped ZnO nanorods for photodegradation of metasystox. Journal of Photochemistry and Photobiology B: Biology, 130: 11-19.
38. Cassano A E, Alfano O M (2000) Reaction engineering of suspended solid heterogenous photocatalytic reactors. Catalysis Today, 58: 167-197.
39. Joseph J M, Destaillats H, Hung H, Hoffmann M R (2000) The sonochemical degradation of azobenzene and related azo dyes: rate enhancements via fenton's reactions. Journal of Physical Chemistry A, 104: 301-307.
40. Spadaro J T, Isabelle L, Renganathan V (1994) Hydroxyl radical mediated degradation of azo dyes: evidence for benzene generation. Environmental Science & Technology, 28: 1389-1393.
41. Galindo C, Jacques P, Kalt A (2000) Photodegradation of the aminobenzene Acid Orange 52 by three advanced oxidation processes: UV/H2O2, UV/TiO2 and VIS/TiO2: comparative mechanistic and kinetic investigations. Journal of Photochemistry and Photobiology A, 130: 35-47.
42. Pala R G S, Metiu H (2007) The structure and energy of oxygen vacancy formation in clean and doped, very thin films of ZnO. Journal of Physical Chemistry C, 111: 12715-12722.